Environ Dev Sustain (2018) 20:2043–2063
https://doi.org/10.1007/s10668-017-9976-y

Integrating spatiotemporal dynamics of natural capital security and urban ecosystem carbon metabolism

Ali Can Demirkesen[1] · **Fatih Evrendilek**[2]

Received: 31 October 2016 / Accepted: 22 May 2017 / Published online: 26 May 2017

Abstract The purpose of the study is to address and quantify the increase in urban expansion and carbon (C) metabolism burden on ecosystem service value (ESV), net ecosystem productivity (NEP), and C storage of urban footprint. Urban footprint is required to meet the demands arising from economic consumption and production as well as waste accumulation and assimilation. Spatiotemporal changes in main land covers (LCs) were detected using remotely sensed data (Landsat 5 and 8, and digital elevation model) between 1987 and 2016. Changes in ESV and C influx, efflux and pools associated with LC dynamics were approximated using global proxies for a western Mediterranean region in Turkey of 54,162 km^2. Urban expansion over the 29-year period decreased ESV by 22% ($7.28 ± 0.4 billion), NEP by 4.3% (2.3 ± 9 Gg C), and total ecosystem C pool by 10.9% (1008.3 ± 1006 Gg C) and led to a 62.8% appropriation of the total NEP (50.1 ± 51 Gg C) of the urban footprint in 2016. The main cause of the environmental degradation across the study region was the loss of the seminatural areas. Our findings emphasize that the deterioration rate of ecosystems should be slowed down by natural capital-friendly decisions and should not exceed rehabilitation rate of damaged ecosystems in the face of rapidly increasing burdens of the cities on their footprint.

Keywords Land-cover change · Sustainability · Environmental monitoring · Ecosystem service value

Electronic supplementary material The online version of this article (doi:10.1007/s10668-017-9976-y) contains supplementary material, which is available to authorized users.

✉ Fatih Evrendilek
fevrendilek@ibu.edu.tr; fevrendilek@yahoo.com

[1] Department of City and Regional Planning, Izmir Institute of Technology, Izmir, Turkey

[2] Department of Environmental Engineering, Abant Izzet Baysal University, Bolu, Turkey

1 Introduction

Natural capital is the inevitable foundation on which socioeconomic systems depend for their survival, well-being and health since its severe scarcity can seriously undermine those (Costanza et al. 2014). Natural capital provides socioeconomic systems with a wide range of ecosystem goods and services (hereafter called ecosystem services) which can be categorized into production, regulation, information, and protection (de Groot et al. 2012). The recognition of this vital role of natural capital has led to a rapidly growing body of research on how to quantify, monitor and secure the natural capital. For example, the ecological footprint was devised as a measure of the amount of biologically productive terrestrial and aquatic areas required to sustain a specific human activity for resource consumptions/productions and waste generations/absorptions (Rees and Wackernagel 1996). This concept has also highlighted that socioeconomic systems can appropriate carrying capacity from not only within but also outside of their own territorial boundaries of natural capital (Ehrlich 1982).

One of the most significant driving forces behind the degradation and destruction of ecosystem services has been the urban expansion and its increased metabolism, with significant implications for natural capital security which encompasses a wide spectrum of securities such as food (biosphere) security, water (hydrosphere) security, energy (geosphere) security, climate (atmosphere) security, and geopolitical (anthroposphere) security. Based on median population projections, the total global human population is most likely to range from 8.1 to 10.6 billion by 2050, with about 6.3 billion expected to inhabit urban areas (UNDP 2015). Globally, the total urban land cover was reported to increase to 58,000 km^2 at an annual rate of ca. 1933 km^2 between 1970 and 2000 and was projected to rise in the range of 430,000–12,568,000 km^2 by 2030 based on a meta-analysis (Seto et al. 2011). In order to reduce our ecological footprint to a globally sustainable level, it makes most sense to secure natural capital with a local focus on urban ecosystems where the most environmentally degradative and destructive changes originate in. The urban ecosystems continue to expand in terms of their spatial extent, population density, metabolism and impervious cover intensity, thus increasing tensions both within themselves and between the urban land and its footprints as well as threatening the Earth's life-support capabilities in urban footprints locally, regionally and globally (Ehrlich et al. 2012).

Wolman (1965) first conceived the concept of urban metabolism to determine per capita inflow and outflow rates for a hypothetical American city (with one million people) using national data on water, food and fuel uses, and generation rates of sewage, waste and air pollutants. Urban metabolism dynamics is generally concerned with the spatiotemporally dynamic quantification of inflow and outflow rates and stocks of energy and biogeochemical cycles for an urban ecosystem (Chen 2015). In practice, however, there still remains an urgent need for an effective tool to integrate spatiotemporal dynamics of natural capital security into land-use planning given the unprecedented rapid growth rates of urbanization and industrialization. In this respect, there exist a limited number of studies about how to harmonize socioeconomic systems and natural capital. For example, various simulation models such as Integrated Valuation of Ecosystem Services and Tradeoffs (InVEST) (Tallis et al. 2013) and land-use scenario dynamics-urban (LUSD-urban) (He et al. 2005) were developed to assist in decision-making process through the quantification and mapping of what-if analyses to explore environmental, economic and social impacts, trade-offs and conflicts of critical policy and management decisions. Global and regional maps of biodiversity hotspots and their ESV estimates were overlapped to assess

opportunities and limitations of their concordance (Chan et al. 2006; Turner et al. 2007). On the other hand, the increasing availability and accessibility of remotely sensed data, and geographic information systems (GIS) have considerably facilitated spatiotemporal analyses of urban land across different resolutions. Therefore, the objective of the present study was to quantify spatiotemporal dynamics and impacts of urban expansion on ESV and C metabolism for both urban land and its footprint in a Mediterranean region of Turkey.

2 Description of the study region

The study region located between 36° and 39°N latitudes and 29°–33°E longitudes occupies a terrestrial extent of ca. 54,162 km^2, with an elevation range of sea level to 3067 m, the peak of Mountain Kizlar Sivrisi (Antalya) of the western Taurus mountain range running parallel to the Mediterranean coast of Turkey (Fig. 1). The administrative units of the study region consist of nine provinces and 59 districts with a total of ca. 9,697,856 people (9,124,144 urban plus 573,712 district dwellers), 12.3% of the national population. Average population density and population growth rate were estimated at 128 people/km^2 and 0.67% over the study region in 2015, and for comparison, were 102 people/km^2 and 0.71% in 2015 at the national scale, respectively (TSI 2015). The prevailing climate is characterized by a Mediterranean warm climate and a temperate semiarid climate with long, dry summers and short rainy seasons during the autumn and winter.

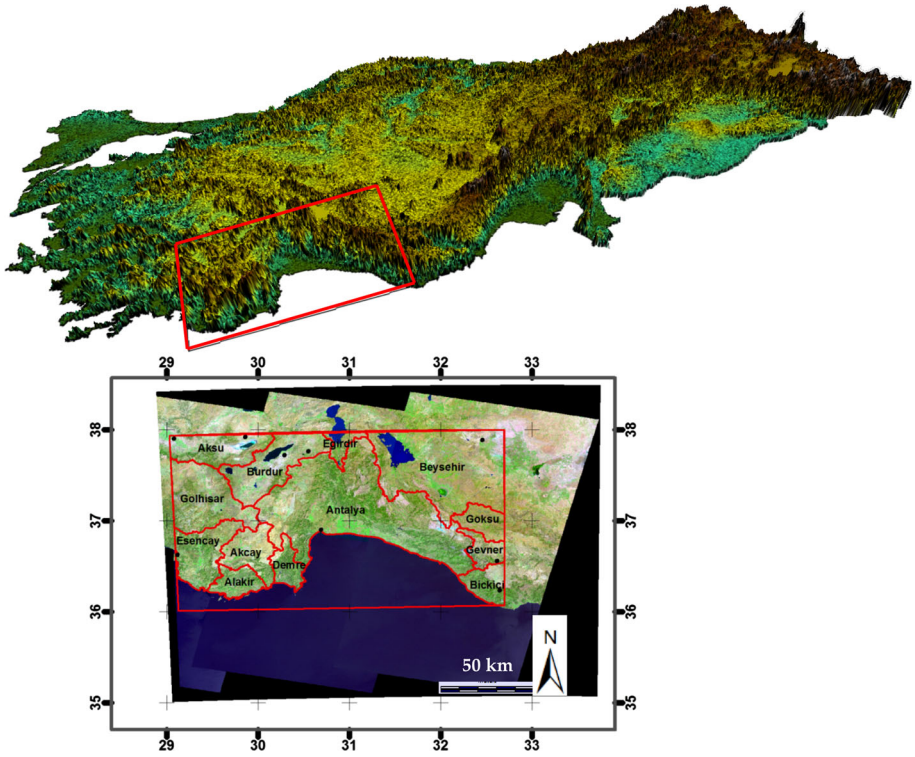

Fig. 1 Location map of the study region with its 13 watersheds in Turkey

According to long-term meteorological data (1968–2013) from 44 stations (TSMS 2013), the mean annual ranges of the major climatic characteristics across the study region included 300–1200 mm for rainfall or precipitation, −4 °C for minimum air temperature to 30.6 °C for maximum air temperature, 5.4–8.5 h for sunshine duration, 10.5–17.5 MJ/m^2/day for solar radiation, 17.9–97.5% for relative humidity, and 988–2190 mm for potential evapotranspiration.

3 Materials and methods

3.1 Data collection

The following three stages were adopted in this study: (1) selection of proxy variables, (2) detection of their spatiotemporal trends, and (3) raster overlay analysis. Natural capital characterization of the study region was carried out using the following remotely sensed variables: (1) digital elevation model (DEM), (2) slope, (3) watershed boundaries, and (4) spatiotemporal trends of NDVI and land surface temperature (LST) in August between 1987 and 2016. Time and space series data of the variables were used to integrate spatiotemporal dynamics of environmental conflicts, ESV, and ecosystem C metabolism into the urban land and its footprint. Finally, a raster overlay analysis was carried out by which the individual maps were compared per pixel to detect the location, severity, amount, and rate of spatiotemporal changes.

3.2 Data processing

Spatiotemporal trends of August LST between 1987 and 2016 over the study region were derived from six frames (paths/rows = 177-178-179/33-34) of each of the two Landsat images: Landsat 5 thematic mapper (TM) in 1987 and Landsat 8 operational land imager (OLI) and thermal infrared sensor (TIRS) in 2016 (http://earthexplorer.usgs.gov/). The Level 1 terrain-corrected Landsat 5 and 8 images were acquired on August 26, 1987 and 2016, respectively, which included atmospheric correction, georectification, and georeferencing to the Universal Transverse Mercator (UTM) projection system with 36 N zone and WGS84 datum.

The dates of Landsat 5 and 8 data were selected according to the least possible degree of cloud cover, cloud shadows or snow cover over the study region. The August LST maps were derived from the thermal infrared (TIR) bands 6 (10.4–12.5 μm) (120 m) and 10 (10.6–11.19 μm) (100 m) of the Landsat 5 and 8 images, respectively, using the following sequential stages: (1) calculation of land surface emissivity (ε), (2) conversion of digital numbers (DN) to spectral radiance (L_λ), (3) conversion of L_λ to brightness temperature (T_b), and (4) conversion of T_b to LST (Sobrino et al. 2004; Weng et al. 2004; Chander et al. 2009; Coll et al. 2010; Barsi et al. 2014). The Landsat TIR data were geometrically transformed to real-world coordinates and converted to 30 m using UTM projection with 36 N zone and WGS84 datum.

3.3 Quantification of environmental conflicts between urban ecosystem and natural capital

The resulting spatiotemporal trends of the differenced August LST images were reclassified identifying natural class breaks that group similar pixel values through the graphical

tool of histogram equalization and were assigned the following five classes of climate change vulnerability index (CCVI): 0 = not vulnerable, 1 = less vulnerable, 2 = moderately vulnerable, 3 = highly vulnerable, and 4 = extremely vulnerable. Hotspots (extremely vulnerable areas) and coldspots (not vulnerable areas) of CCVI were determined as areas where the highest increases and no or slight changes in the August LST temperature between 1987 and 2016 occurred, respectively. Slope, watershed boundaries, and DEM classification were derived from the Advanced Spaceborne Thermal Emission and Reflection Radiometer (ASTER) Global Digital Elevation Model (GDEM) (30-m resolution) acquired from http://gdex.cr.usgs.gov/gdex/. A total of 13 watersheds were delineated in the study region as the most natural spatial scale for the quantification of harmonization between urban metabolism and its footprint. A shapefile consisting of administrative boundaries (province and district) of the study region was also obtained as ancillary data from the General Command of Mapping (http://www.hgk.msb.gov.tr/).

29-year spatiotemporal trends of LCs were derived from the two images identifying the following five terrestrial LCs: built-up land (BUL), agricultural land (AL), seminatural land (SNL), water body (WB), and bareland (BL). The multispectral image LC classification was performed using the maximum likelihood algorithm. Accuracy of the LC classifications on a per pixel basis was measured using the matrix of producer's and user's accuracies, and Kappa statistics (Demirkesen 2008). All spatiotemporal analyses and statistics including the final CCVI calculation were calculated using ArcGIS 10.4 and IDRISI Selva 17.0 software.

Agricultural land was defined to include cropland, pasture, orchards, groves, vineyards, and nurseries and was classified as prime farmland according to the slope classes of 0°–6° and other agricultural land according to the slope classes of 6°–12° and >12°, respectively. Seminatural land was defined to include Mediterranean and warm-temperate semiarid evergreen forests, shrubland, grassland, and environmental protection areas according to NDVI value $\geq$0.4. Buffer zones against flood and geologic hazards, and deterioration of coastal land and water resources were created to avoid environmental conflicts in the face of urban encroachments. Buffer zones were determined isolating a safe minimum area of specified widths of 60 m on the side of the lakes, and each side of the river, of 300 m along the coastline, and of 90 m on each side of the faults. Built-up land included both urban settlements and roads. Urban encroachments into prime farmland, other agricultural land, buffer zones, and the classes of CCVI in this study were considered to be the main environmental conflicts not appreciating natural capital security and were detected between 1987 and 2016.

3.4 Quantification of ecosystem service value

An approximation of annual ESV for the study region was carried out relating the observed LC dynamics to the 2011 global averages of unit values for a total of 17 ecosystems services according to proxy biomes reported in Table 1 by Costanza et al. (2014) and de Groot et al. (2012) as follows:

$$\mathrm{ESV} = \sum(\mathrm{A}_i \times \mathrm{UV}_i), \tag{1}$$

where ESV denotes the total mean annual ESV ($/year) expressed in 2007$US, A_i is the area (km^2) of LC type i, and UV_i is the global average unit value ($/km^2/year) of a total of 17 ecosystems services for a proxy LC type I reported in Table 1. Mean UV_i was used when multiple proxy values were available for each LC of the study region. Uncertainties

Table 1 Global average unit values (UV, $/km^2/year) and standard deviations (SD) in 2011 of a total of 17 ecosystem services expressed in 2007 $US for land covers (LCs) used as proxies in this study

LC	Urban footprint				BUL
UV	SNL	AL	WB	BL	
Proxy biome	Temperate forest; grass; floodplain	Cropland, rangeland	Lakes/ rivers	Ice/rock/sparse vegetation	Urban
References	Costanza et al. (2014)	Costanza et al. (2014)	Costanza et al. (2014)	Costanza et al. (2014)	Costanza et al. (2014)
Proxy 2011 UV (2007$/ km^2/year)	313,700; 416,600; 2,568,100	556,700; 416,600	1,251,200	2598	666,100
References	Costanza et al. (2014)	Costanza et al. (2014)	Costanza et al. (2014)	Costanza et al. (1997) and Portela and Rademacher (2001)	Costanza et al. (2014)
Proxy SD	543,700; 386,000; 504,500	386,000	277,100	0	118,936
References	de Groot et al. (2012)	de Groot et al. (2012)	de Groot et al. (2012)	Costanza et al. (1997) and Portela and Rademacher (2001)	Costanza et al. (1997), Shrestha and Loomis (2003), Li et al. (2010) and Liu et al. (2010)
Adopted UV (2007$/ km^2/year)	1,099,467	486,650	1,251,200	2598	666,100
Adopted SD	504,500	386,000	277,100	0	118,936

associated with ESV estimates for each LC of the study region were quantified using proxy standard deviations (SD) where possible based on related literature.

3.5 Quantification of urban ecosystem carbon metabolism

Such components as influxes, effluxes, net ecosystem exchange, and pools of C cycle in the study region were approximated using global averages reported in related literature. Carbon inflows not only by urban vegetation but also by vegetation of the urban footprint considered in this study consisted of net primary productivity (NPP) and gross primary productivity (GPP). Total GPP is the sum of NPP and autotrophic respiration (R_a), or as the sum of net ecosystem productivity (NEP) and ecosystem respiration (R_e). Carbon efflux taken into account in this study consisted of R_e as the sum of R_a and soil (R_h) respiration for the urban footprint (non-urban LCs) and additionally included human respiration, waste decomposition at landfills, burning of fossil fuels for energy needs, and urban expansion into urban footprint for the urban land. Global averages of GPP, NPP, NEP, and R_e values (g C/m^2/year) for Mediterranean and warm-temperate semiarid evergreen vegetation of SNL were derived from Luyssaert et al. (2007), Haberl et al. (2007), Gilmanov et al. (2010), and Raich et al. (1991) as proxies for the present study (Table 2). Carbon pools

were assumed to include the stocks of aboveground biomass C (AGC), belowground biomass C (BGC), soil organic C (SOC), and litter organic C (LOC) for the urban footprint and the additional stocks of landfill waste C (LWC), building C (BC), and human C (HC) for the urban land (Table 2). Carbon fluxes and pools and their uncertainties in this study were quantified using means of high- and low-bound estimates or SD wherever possible based on related literature.

Urban appropriation of its hinterland natural capital is needed to sustain urban ecosystems and was referred to as appropriated urban footprint (AUF) in this study. Appropriated urban footprint was quantified as the sum of human-induced losses of NEP due to both destructive (quantitative) and degradative (qualitative) changes in SOC, AGC, and BGC (by harvests, biomass burning, and LULC conversions) based on the concept of human appropriation of NPP (HANPP). Estimates of AUF were calculated modifying the equation reported by Churkina (2016) thus:

$$\mathrm{AUF} = f\mathrm{HANPP}_{\mathrm{urb}} \times \frac{\mathrm{NEP}}{\mathrm{NPP}} \times \mathrm{HANPP}_{\mathrm{uv}} \times \mathrm{Area}_{\mathrm{urb}}, \quad (2)$$

where $f\mathrm{HANPP}_{\mathrm{urb}}$ is the fraction of HANPP caused by urban ecosystems (%). The low, best, and high values of $f\mathrm{HANPP}_{\mathrm{urb}}$ were assumed as 6.2, 33.1, and 60%, respectively, based on the low and high values by Churkina (2016) and Plutzar et al. (2016) who reported to vary between 50 and 70% globally and between 2.7 and 9.7% in the EU, respectively. NEP/NPP is a study region-specific conversion factor from NPP to NEP for $\mathrm{HANPP}_{\mathrm{uv}}$. $\mathrm{HANPP}_{\mathrm{uv}}$ is the unit value (t C/ha/year) of HANPP which was used as the EU-specific $\mathrm{HANPP}_{\mathrm{uv}}$ (3 ± 1 t C/ha/year) reported by Plutzar et al. (2016) instead of using the global $\mathrm{HANPP}_{\mathrm{uv}}$ average (1.2 t C/ha/year, or 15.6 Pg C/year) (Pg $= 10^{15}$ g) stated by Haberl et al. (2007). $\mathrm{Area}_{\mathrm{urb}}$ is the study region-specific urban area (ha).

4 Results and discussion

4.1 Spatiotemporal changes in environmental conflicts

Among all the LC expansions, the urban expansion across the study region experienced the maximum increase by 137% over the 29-year period at an annual rate of 10.3 km^2 (Table 3). The only decrease took place with SNL by 48% (Table 3; Fig. 2). The minimum increase occurred by 10% with the LC class of water body (rivers and lakes) (Table 3). Urban encroachments into the prime farmland, the other agricultural land, the buffer zones, and the classes of CCVI were considered to be the critical environmental conflicts that threatened not only the well-being and health of the urban ecosystem but also its footprint (natural capital security) and were also detected over the period of 1987–2016 (Figs. 3, 4, 5). The entire area for each of the buffer zones in 2016 constituted 298 km^2 along the shoreline, 339.6 km^2 around the water bodies, and 196.3 km^2 around the faultlines (Fig. 3). The total area of the urban encroachments into the buffer zones in 2016 was estimated at 18.8 km^2, 4.3, 27.7, and 68.1% of which were related to the faultlines, the water body, and the coastline, respectively (Fig. 3). The entire agricultural land in the study region covered 18,766 km^2 (35% of the study region) which were partitioned into 1795 km^2 for the prime farmland with a slope range of 0°–6°, and 3152 and 13,819 km^2 for the remaining agricultural land with a slope range of 6°–12°, and >12°, respectively (Fig. 4). The 29-year urban encroachment into the agricultural land amounted to a total of 241.9 km^2 18.3, 31.2, and 50.5% of which corresponded to the prime farmland, and the

Table 2 Mean values (t C/ha/year) of main components of carbon (C) cycle for land covers (LCs) in this study

LC	Urban footprint				BUL
C component	SNL	AL	WB	BL	
C inflow					
GPP	10.6 ± 3.4	12.3 ± 3.7	6.1 ± 1.1	0.23	4.2 ± 2.4
References	Luyssaert et al. (2007) and Gilmanov et al. (2010)	Gilmanov et al. (2010)	Pace and Prairie (2005) and Battin et al. (2008)	Thomazini et al. (2016)	Peters and McFadden (2012)
NPP	4.4 ± 2.2	4.0	2.7	0.12 ± 0.03	2.0 ± 0.4
References	Luyssaert et al. (2007), Haberl et al. (2007) and Raich et al. (1991)	Haberl et al. (2007)	Lewis (2011)	Eisfelder et al. (2012)	Nowak et al. (2013)
C outflow					
R_e	9.9 ± 2.84	9.7 ± 2.4	12.1 ± 1.6	0.91	44.2 ± 20.4
References	Luyssaert et al. (2007) and Gilmanov et al. (2010)	Gilmanov et al. (2010)	Pace and Prairie (2005) and Battin et al. (2008)	Thomazini et al. (2016)	Liu et al. (2010), Crawford and Christen (2015) and Liu et al. (2012)
NEP	0.7 ± 0.6	2.6 ± 1.3	0.7 ± 0.8	−0.23	−41.5 ± 20
References		Gilmanov et al. (2010)	Butman et al. (2016)	Thomazini et al. (2016)	
C pool					
AGC	61.1 ± 36.8	15	0.079 ± 0.078	30.5 ± 18.4	21.6 ± 8.9
BGC	27.4 ± 19.7	1.5	Not applicable	13.7 ± 9.8	64.1 ± 8.6
References	Luyssaert et al. (2007)	Jackson et al. (1996) and Jobbagy and Jackson (2000)	Lacroix et al. (1999)		Pouyat et al. (2006)
SOC	117.0 ± 63.0	112.0 ± 7.0	495.0 ± 215.0	33.0 ± 9.3	70.0 ± 7.8
References	Jobbagy and Jackson (2000)	Jobbagy and Jackson (2000)	Anderson et al. (2009) and Tranvik et al. (2009)	Pouyat et al. (2006)	Pouyat et al. (2006)
LOC	32.3	15.6		0.8 ± 0.3	0.4 ± 0.03

Table 2 continued

LC	Urban footprint				BUL
C component	SNL	AL	WB	BL	
References	Brovkin et al. (2012) and Potter and Klooster (1997)	Brovkin et al. (2012) and Potter and Klooster (1997)		Jo and McPherson (1995)	Kaye et al. (2005)
LWC					162.0
BC					63.5
HC					1.1
References					Churkina (2016)

Negative values denote net C efflux

Table 3 Amount and rate of spatiotemporal changes in land covers (LCs) of the study region between 1987 and 2016, and accuracy metrics of Landsat-derived LC classification

LC	1987 (km^2)	% of total land	2016 (km^2)	% of total land	Amount of change		Rate of change	PA (%)	UA (%)	Kappa (%)
					(km^2)	(%)	(km^2/year)			
AL	19,008.3	35.0	25,779.9	47.5	6771.7	36	233.5	85	85	85
WB	919.1	1.9	1007.1	2.0	88.1	10	3.0	98	98	98
SNL	20,630.1	38.0	10,721.6	19.8	−9908.6	−48	−341.7	90	90	90
BUL	217.2	0.4	515.2	0.9	298.0	137	10.3	95	95	95
BL	13,387.6	24.7	16,138.5	29.7	2750.9	21	94.9	85	85	85
Total	54,162.3									

Negative values denote a decrease

PU producer's accuracy, *UA* user's accuracy

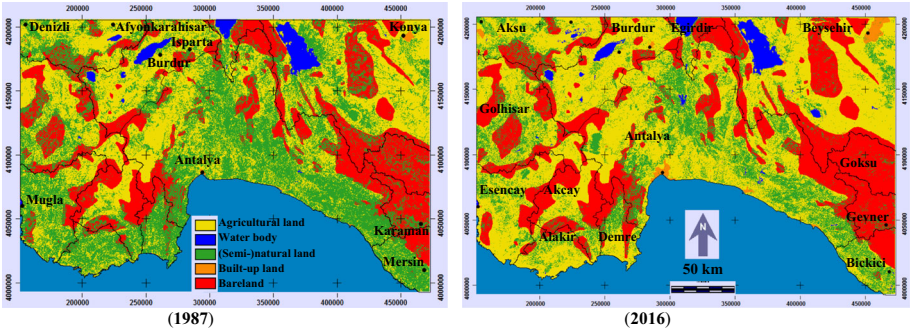

Fig. 2 Changes in land covers (LCs) between 1987 and 2016 according to 13 watersheds of the study region used to elucidate spatiotemporal dynamics of urban expansions, environmental conflicts, ecosystem service values, and ecosystem C metabolism for urban land and its footprint. The names of nine provinces and 13 watersheds are presented in the 1987 and 2016 maps, respectively

other agricultural land with a slope range of 6°–12°, and >12°, respectively (Fig. 4). Our CCVI showed that the areas of the study region ranked in not, less, moderately, highly and extremely vulnerable were 51,892, 347, 278, 1197 and 18 km^2, respectively (Fig. 5). The total area of the urban encroachment according to the CCVI classes was 27.7 km^2, 0.4, 1.1, and 98.5% of which belonged to the classes of less, extremely and highly vulnerable, respectively (Fig. 5).

The 29-year spatiotemporal changes in LCs, and urban expansions into environmentally sensitive and risky zones, the agricultural land, and the five classes of the CCVI are presented in Figs. 2, 3, 4, and 5, respectively, according to the 13 watersheds. The loss of SNL was concentrated primarily in the watersheds directly adjacent to the Mediterranean coastline and secondarily in Beysehir and Burdur watersheds (Fig. 2). The highest increase in the urban expansion occurred with Antalya (Antalya watershed) and Konya (Beysehir watershed). The maximum shares of the urban encroachments belonged to Antalya and Bickici watersheds for the shoreline, to Beysehir watershed for the water body and to Antalya watershed for the faultline (Fig. 3). Beysehir and Antalya watersheds were

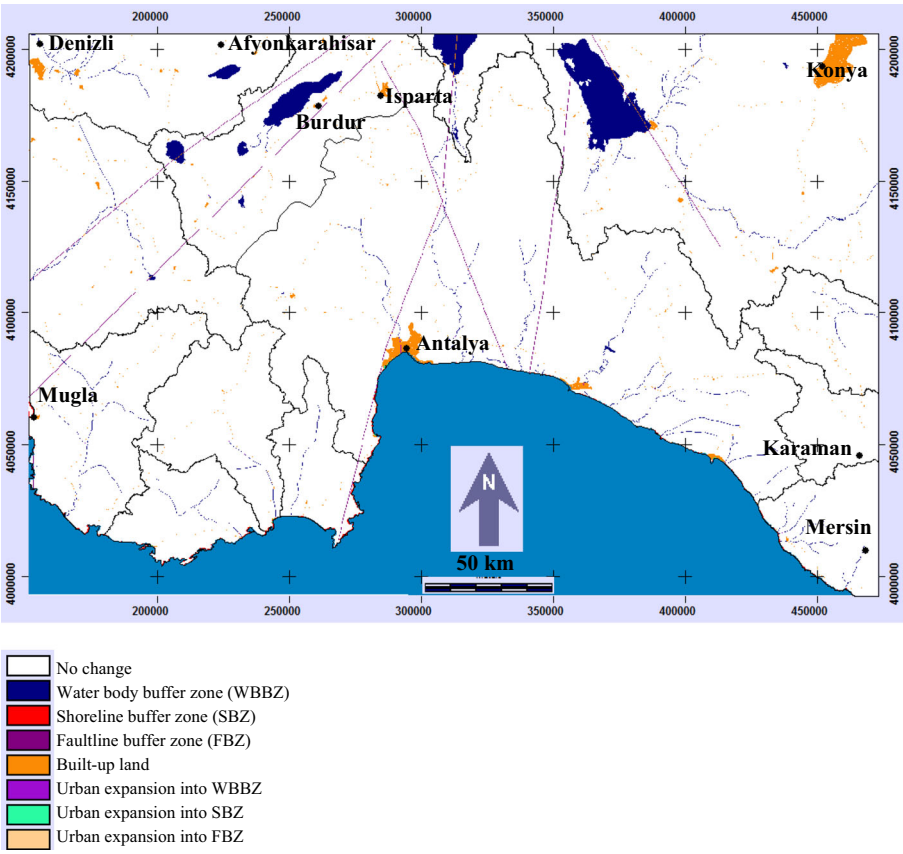

Fig. 3 Urban expansion into environmentally sensitive and risky zones over the period of 1987–2016 according to 13 watersheds of the study region used to elucidate environmental conflicts between urban ecosystem and its footprint

responsible for most of the encroachment into the prime farmland (Fig. 4) and were found to contain all the extremely vulnerable areas (hotspots) and most of the highly vulnerable areas of the CCVI, respectively (Fig. 5).

4.2 Spatiotemporal changes in ecosystem service value

The aggregate regional monetary value including both market and non-market values expressed in 2007 $US was approximated for a total of 17 ecosystem services of the study region in 1987 and 2016 (Table 4). Spatiotemporal changes in the ESV of the (non-)urban LCs in the study region were estimated multiplying the area of each of the five LC classes in 1987 and 2016 by the related unit value in Table 1. The total ESV of the study region was found as $25.98 ± 17.6 billion in 2016 and declined by 22% ($7.28 ± 0.4 billion) at an annual rate of $251 million over the 29-year period (Table 4). The decrease in SNL by 48% alone resulted in this ESV loss despite the increased ESV of the other LCs (Table 4).

Likewise, the total global monetary value expressed in 2007 $US was on average estimated at $124.8 trillion/year as a function of a total of 17 ecosystem services in 2011

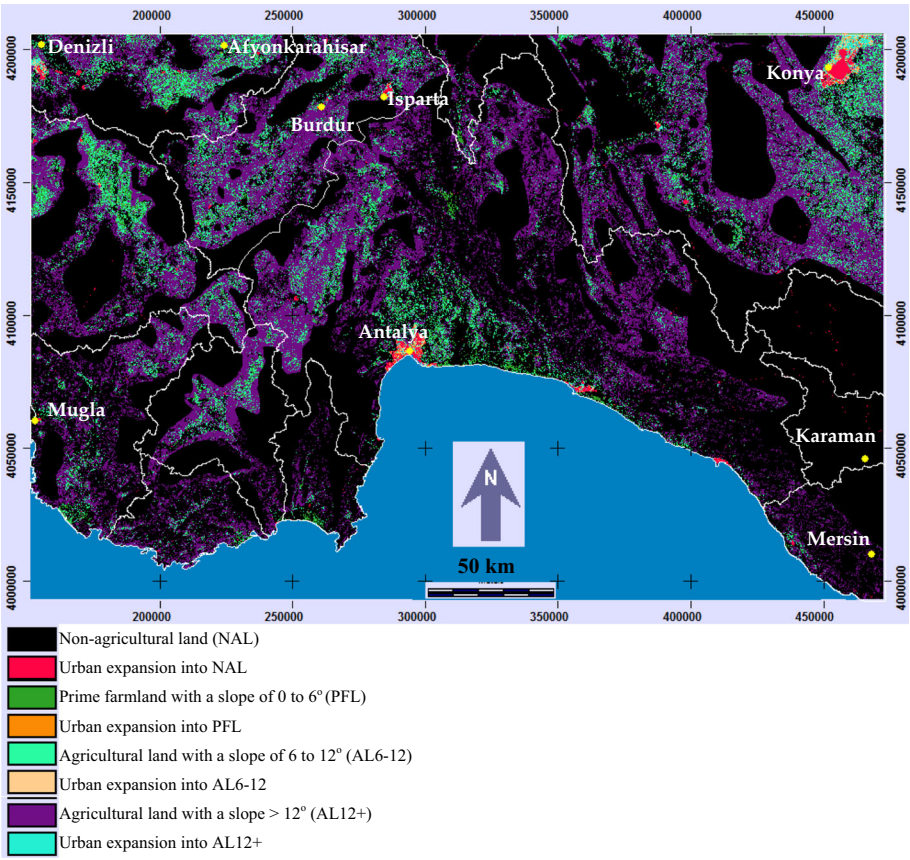

Fig. 4 Urban expansions into prime farmland, other agricultural land, and non-agricultural land between 1987 and 2016 according to 13 watersheds of the study region used to elucidate environmental conflicts between urban ecosystem and its footprint

for 16 main biomes by Costanza et al. (2014) and at $165 trillion/year as a function of a total of 22 ecosystem services in 2012 for 10 main biomes by de Groot et al. (2012). The total regional ESV estimate in 2016 of this study constituted 0.2‰ of the total global ESV estimate of $124.8 trillion/year by Costanza et al. (2014). Given the total land area of $51{,}625 \times 10^4$ km^2 used in the total global ESV estimate by Costanza et al. (2014), the unit ESV estimate across all the ecosystem types was 2.54 times higher in the study region ($614,115/km^2/year) than globally ($241,743/km^2/year).

4.3 Spatiotemporal changes in ecosystem carbon metabolism of urban land and its footprint

4.3.1 Influx, efflux, and net ecosystem exchange of carbon

The loss of SNL more than offset the increase in C sequestration by GPP or NPP associated with the increased areas of the other LCs over the 29-year period (Tables 5, 6) and caused an overall decline by 19.3 ± 8 and 15.3 ± 3 Gg C for the total GPP and NPP, respectively

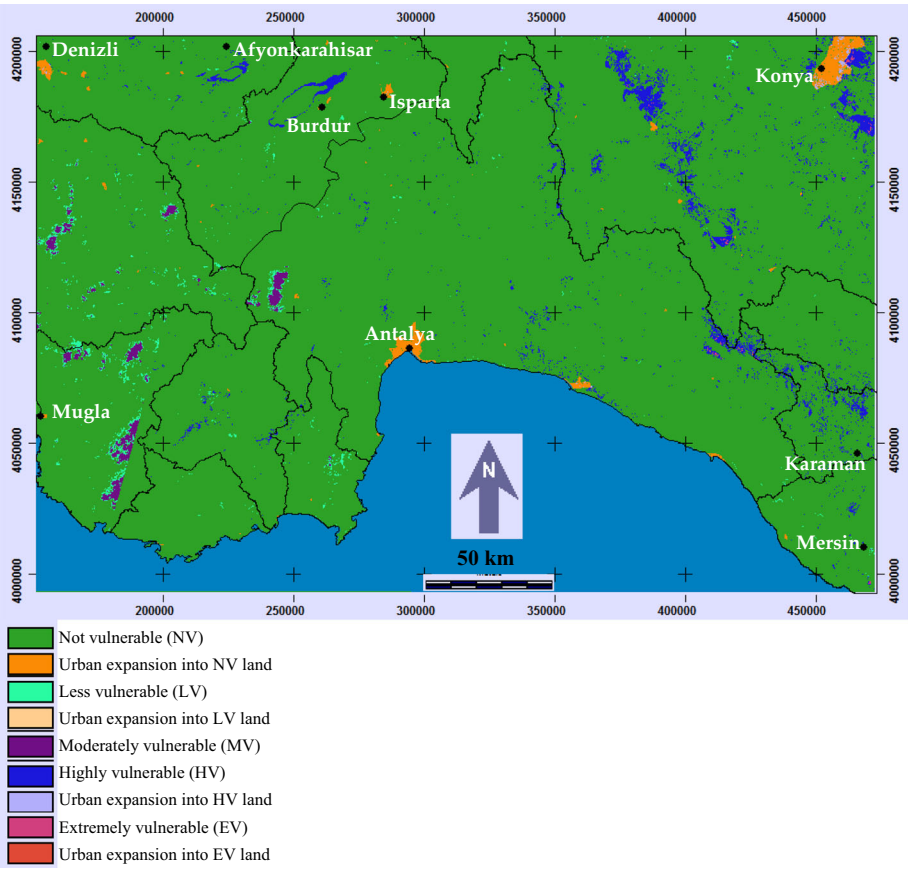

Fig. 5 Urban expansion into the five classes of climate change vulnerability index (CCVI) between 1987 and 2016 according to 13 watersheds of the study region used to elucidate environmental conflicts between urban ecosystem and its footprint

(Table 7). The agricultural land and SNL dominated C removal through GPP and NPP from the atmosphere in 1987, respectively, whereas the dominance of C removal by both GPP and NPP shifted to the agricultural land alone in 2016. Urban vegetation accounted for 0.5% of the total GPP, while urban vegetation and soil contributed to 5.6% of the total R_e across the LCs in 2016.

Overall C release by R_e from the LCs to the atmosphere decreased by 15.7 ± 5 Gg C over the same period (Table 7). The second highest increase in R_e over the 29-year period occurred with the built-up land after the agricultural land. The overall NEP for the study region decreased from 52.4 ± 42 Gg C/year in 1987 to 50.1 ± 51 Gg C/year in 2016 during which the agricultural land and the water bodies were the only LCs with the increased NEP by 17.6 ± 9 and 0.1 ± 0.1 Gg C/year, respectively. This big difference between urban GPP and R_e caused the urban ecosystem to be responsible for the highest decrease by 21% in the total NPP in 2016. Unlike the urban land, the agricultural land exerted the greatest influence on the increased NEP over the 29-year period. Despite the

Table 4 Amount and rate of spatiotemporal changes in ecosystem service value (ESV) according to land covers (LCs) of the study region between 1987 and 2016

LC	Year	ESV	SD	Amount of change		Rate of change
		(10^9 × 2007$)		(10^9 × 2007$)	%	(10^6 × 2007$)
SNL	1987	22.68	10.41	−10.9 ± 3.1	−48	−375.7
	2016	11.79	7.34			
AL	1987	9.25	7.34	3.3 ± 2.6	36	113.6
	2016	12.55	9.95			
WB	1987	1.15	0.25	0.11 ± 0.02	10	3.8
	2016	1.26	0.28			
BL	1987	0.03	0.0	0.01 ± 0.0	21	0.2
	2016	0.04	0.0			
BUL	1987	0.14	0.03	0.2 ± 0.04	137	6.8
	2016	0.34	0.06			
Total	1987	33.26	18.0	−7.28 ± 0.4	−22	−251.1
	2016	25.98	17.6			

Negative values denote a decrease

decreasing NEP by 2.3 Gg C over the study period, the study region acted as a C sink. Ecosystem respiration of the global urban footprint (outside of the city limits) from all the activities by urban dwellers including production and consumption of food, fiber, and energy was estimated to constitute 10–35% of the global terrestrial R_e (107.2 Pg C/year) (Churkina 2016).

4.3.2 Ecosystem carbon pools

Total ecosystem C pool considered in this study consisted of the individual stocks of AGC, BGC, SOC, and LOC for the urban footprint and included the additional LWC, BC, and HC stocks for the urban land. The entire study region lost a total ecosystem C stock of 1008.3 ± 1006 Gg C over the study period of 29 years due to the loss of SNL (Table 7). The biggest share (41%) of this loss stemmed from the loss of AGC storage across the LCs. The primary role in the maintenance of the total ecosystem C storage was also shifted from SNL in 1987 to the agricultural land in 2016 (Tables 5, 6). The urban landfill wastes (1.0%), urban buildings (small and slow C sequestration in concrete buildings through carbonation) (0.4%), and urban dwellers (0.01%) explained 1.4% of the total ecosystem C pool of 8219.0 ± 2301 Gg C in 2016. The SOC pool to a depth of 0–1 m (sediment C pool in case of water body) was greater than the total biomass C pool of AGC plus BGC (sum of phytoplankton and zooplankton biomass C in case of water body) for SNL and agricultural lands, and the water bodies in 1987 and 2016 unlike for the bareland and the urban land. The most recent global estimates of urban C storage ranged from 4 to 29 Pg C (excluding LWC) or 59 Pg C (including LWC) with the best estimate of 16 Pg C based on a global assessment by Churkina (2016) and from 4.4 to 56.4 Pg C based on the product of the minimum and maximum global urban extents (276,000–3,524,000 km^2) by the global average of urban-specific C density (16 kg C/m^2) by Zhao et al. (2013).

Table 5 Mean fluxes (Gg C/year) and pools (Gg C) (Gg = 10^9 g) of C metabolism of urban ecosystem and its footprint according to land covers (LCs) of the study region in 1987

LC C cycle		Urban footprint				BUL	Total
		SNL	AL	WB	B		
Influx	GPP	218.7 ± 70	233.8 ± 70	5.6 ± 1	3.1	0.9 ± 0.5	462.1 ± 142
	NPP	90.8 ± 45	76.0	2.5	1.6 ± 0.4	0.4 ± 0.1	171.3 ± 46
Efflux	R_e	204.2 ± 58	184.4 ± 46	11.1 ± 2	12.2	9.6 ± 4	421.5 ± 109
NEP		14.4 ± 12	49.4 ± 25	0.6 ± 1	−3.1	−9.0 ± 4	52.4 ± 42
Pool	AGC	1260.5 ± 759	285.1	0.1 ± 0.1	408.3 ± 246	4.7 ± 2	1958.7 ± 1007
	BGC	565.3 ± 406	28.5		183.4 ± 131	13.9 ± 2	791.1 ± 539
	SOC	2413.7 ± 1300	2128.9 ± 133	454.9 ± 198	441.8 ± 124	15.2 ± 2	5454.6 ± 1757
	LOC	666.4	296.5		10.7 ± 4	0.1 ± 0.01	973.7 ± 4
	LWC					35.2	35.2
	BC					13.8	13.8
	HC					0.2	0.2
Total pool		4905.8 ± 2465	2739.1 ± 133	455.0 ± 198	1044.2 ± 506	83.1 ± 5	9227.3 ± 3308

Negative values denote a decrease

Table 6 Mean fluxes (Gg C/year) and pools (Gg C) (Gg = 10^9 g) of C metabolism of urban ecosystem and its footprint according to land covers (LCs) of the study region in 2016

LC C cycle		Urban footprint				BUL	Total
		SNL	AL	WB	B		
Influx	GPP	113.6 ± 36	317.1 ± 95	6.1 ± 1	3.7	2.2 ± 1	442.8 ± 134
	NPP	47.2 ± 24	103.1	2.7	1.9 ± 0.5	1.0 ± 0.2	156.0 ± 24
Efflux	R_e	106.1 ± 30	250.1 ± 62	12.2 ± 2	14.7	22.8 ± 11	405.9 ± 104
NEP		7.5 ± 6	67.0 ± 34	0.7 ± 1	−3.7	−21.4 ± 10	50.1 ± 51
Pool	AGC	655.1 ± 395	386.7	0.1 ± 0.1	492.2 ± 297	11.1 ± 5	1545.2 ± 696
	BGC	293.8 ± 211	38.7		221.1 ± 158	33.0 ± 4	586.6 ± 374
	SOC	1254.4 ± 675	2887.4 ± 180	498.5 ± 217	532.6 ± 150	36.1 ± 4	5208.9 ± 1227
	LOC	346.3	402.2		12.9 ± 5	0.2 ± 0.02	761.6 ± 5
	LWC					83.5	83.5
	BC					32.7	32.7
	HC					0.6	0.6
Total pool		2549.6 ± 1281	3714.9 ± 180	498.6 ± 217	1258.8 ± 610	197.2 ± 13	8219.0 ± 2301

Negative values denote a decrease

Table 7 Spatiotemporal changes in mean fluxes (Gg C/year) and pools (Gg C) (Gg = 10^9 g) of C metabolism of urban ecosystem and its footprint according to land covers (LCs) of the study region between 1987 and 2016[1]

LC C cycle		Urban footprint				BUL	Total
		SNL	AL	WB	B		
Influx	GPP	−105.0 ± 34	83.3 ± 25	0.5 ± 0.1	0.6	1.3 ± 1	−19.3 ± 8
	NPP	−43.6 ± 22	27.1	0.2	0.3 ± 0.1	0.6 ± 0.1	−15.3 ± 22
Efflux	R_e	−98.1 ± 23	65.7 ± 16	1.1 ± 0.1	2.5	13.2 ± 6	−15.7 ± 5
NEP		−6.9 ± 6	17.6 ± 9	0.1 ± 0.1	−0.6	−12.4 ± 6	−2.3 ± 9
Pool	AGC	−605.4 ± 365	101.6	0.01 ± 0.01	83.9 ± 51	6.4 ± 3	−413.5 ± 311
	BGC	−271.5 ± 195	10.2		37.7 ± 27	19.1 ± 3	−204.5 ± 166
	SOC	−1159.3 ± 624	758.4 ± 47	43.6 ± 19	90.8 ± 26	20.9 ± 2	−245.6 ± 530
	LOC	−320.0	105.6		2.2 ± 0.8	0.1 ± 0.01	−212.1 ± 1
	LWC					48.3	48.3
	BC					18.9	18.9
	HC					0.3	0.3
Total pool		−2356.3 ± 1184	975.8 ± 47	43.6 ± 19	214.6 ± 104	114.0 ± 7	−1008.3 ± 1006

Negative values denote a decrease

4.4 Spatiotemporal changes in appropriated urban footprint

The urban ecosystem in this study was assumed to be responsible for a minimum of 6.2% to a maximum of 60% (with a mean of 33.1%) of $HANPP_{uv}$ based on the most recent estimates of 3.0 ± 1 t C/ha/year for $HANPP_{uv}$, 2.7–9.7% for the minimum $fHANPP_{urb}$ for the EU in 2006 by Plutzar et al. (2016), and of 50–70% for the maximum $fHANPP_{urb}$ globally in 2000 by Haberl et al. (2007). The AUF value across the study region was estimated at 13.3 ± 10.8 Gg C in 1987 and 31.5 ± 25.6 Gg C in 2016. The AUF estimates in 1987 and 2016 accounted for 25.3 and 62.8% of the total NEP values (52.4 ± 42 and 50.1 ± 51 Gg C) in 1987 and 2016, respectively. Over the 29-year period, the AUF rose by 18.2 ± 14.8 Gg C at a rate of 0.63 ± 0.51 Gg C/year. If the current AUF trends of the study region persist with the entire regional NEP in 2016 remaining the same, then it would take about 33 years in order for the entire urban footprint to be appropriated by the cities. This suggests that the loss and degradation rates of the local non-urban ecosystems within the urban footprint should be slowed down by the harmonization of urban expansion and natural capital security and should not exceed rehabilitation rate of damaged ecosystems, in particular, given the rapidly increasing demands of the cities for their footprint locally. Globally, GPP by the urban footprint was reported to amount to 22 and 24% of the entire terrestrial GPP (112 Pg C/year) and C emissions (117 Pg C/year) in 2006 (Churkina 2016).

5 Conclusion

The novelty of the present study lies, for the first time, in its spatiotemporally dynamic analyses on a regional scale of (1) urban expansion into environmentally vulnerable and risky footprint; (2) ESV of natural capital and (3) ecosystem C metabolism (C fluxes and pools) for urban land and its footprint; and (4) urban appropriation of C metabolism in its footprint. Our spatiotemporal analysis showed a significantly decreasing trend in the overall ESV between 1987 and 2016 by 22% ($7.28 ± 0.4 billion in 2007$ value) primarily caused by the loss of SNL, thus indicating the severity of the environmental degradation and destruction of the study region. During this period, all the LC areas expanded with the highest increase exhibited by the rapid urban expansion by 137% whose increasing ESV rate of $6.8 million/year was ranked second. However, the highest increasing rate ($113.6 million/year) of the ESV occurred with the agricultural land followed by the bareland and the inland water bodies. LC-induced impacts on the urban footprint over the 29-year period led to the decreases in NEP by 4.3% (2.3 ± 9 Gg C) and a total ecosystem C pool by 10.9% (1008.3 ± 1006 Gg C). Urban-related activities were estimated to control and appropriate 62.8% of the total NEP (50.1 ± 51 Gg C) in 2016. The ecosystem analysis of temporal as well as spatial changes in C metabolism of the urban land and the urban footprint, urban appropriation of C metabolism in the urban footprint, ESV, environmental conflicts, and their interacting hotspots and coldspots may provide significant contributions to how to integrate natural capital security into socioeconomic development policies across a wide range of spatiotemporal scales. In particular, the direction of local urban growth and development can be adjusted in a natural capital-friendly way. As with the other studies in the related literature, the proxies and the assumptions were adopted in this study, due to data limitations and/or lack of local estimates of ESV, and C fluxes and pools. In the future studies, the integration of field data

collection from different biomes into remotely sensed data remains to be explored to better understand and predict spatiotemporal dynamics of how urban expansion affects ESV and C cycle within the urban footprint in a changing global climate.

Acknowledgements We are grateful to three anonymous reviewers whose constructive comments significantly improved an earlier version of the article. We would like to thank Izmir Institute of Technology and Abant Izzet Baysal University for supporting this study.

References

Anderson, N. J., D'Andrea, W., & Fritz, S. C. (2009). Holocene carbon burial by lakes in SW Greenland. *Global Change Biology, 15,* 2590–2598.

Barsi, J. A., Schott, J. R., Hook, S. J., Raqueno, N. G., Markham, B. L., & Radocinski, R. G. (2014). Landsat-8 thermal infrared sensor (TIRS) vicarious radiometric calibration. *Remote Sensing, 6,* 11607–11626.

Battin, T. J., Kaplan, L. A., Findlay, S., Hopkinson, C. S., Marti, E., Packman, A. I., et al. (2008). Biophysical controls on organic carbon fluxes in fluvial networks. *Nature Geoscience, 1,* 95–100.

Brovkin, V., van Bodegom, P. M., Kleinen, T., Wirth, C., Cornwell, W. K., Cornelissen, J. H. C., et al. (2012). Plant-driven variation in decomposition rates improves projections of global litter stock distribution. *Biogeosciences, 9,* 565–576.

Butman, D., Stackpoole, S., Stets, E., McDonald, C. P., Clow, D. W., & Striegl, R. G. (2016). Aquatic carbon cycling in the conterminous United States and implications for terrestrial carbon accounting. *Proceedings of the National Academy of Sciences of the United States of America, 113,* 58–63.

Chan, K. M. A., Shaw, M. R., Cameron, D. R., Underwood, E. C., & Daily, G. C. (2006). Conservation planning for ecosystem services. *PLoS Biology, 4,* e379.

Chander, G., Markham, B. L., & Helder, D. L. (2009). Summary of current radiometric calibration coefficients for Landsat MSS, TM, ETM +, and EO-1 ALI sensors. *Remote Sensing of Environment, 113,* 893–903.

Chen, B. (2015). Integrated ecological modelling for sustainable urban metabolism and management. *Ecological Modelling, 318,* 1–4.

Churkina, G. (2016). The role of urbanization in the global carbon cycle. *Frontiers in Ecology and Evolution, 3,* 144.

Coll, C., Galve, J. M., Sanchez, J. M., & Caselles, V. (2010). Validation of Landsat-7/ETM+ thermal-band calibration and atmospheric correction with ground-based measurements. *IEEE Transactions on Geoscience and Remote Sensing, 48,* 547–555.

Costanza, R., d'Arge, R., de Groot, R., Farber, S., Grasso, M., Hannon, B., et al. (1997). The value of the world's ecosystem services and natural capital. *Nature, 387,* 253–260.

Costanza, R., de Groot, R., Sutton, P., van der Ploeg, S., Anderson, S. J., Kubiszewski, I., et al. (2014). Changes in the global value of ecosystem services. *Global Environmental Change, 26,* 152–158.

Crawford, B., & Christen, A. (2015). Spatial source attribution of measured urban eddy covariance CO_2 fluxes. *Theoretical and Applied Climatology, 119,* 733.

de Groot, R., Brander, L., van der Ploeg, S., Costanza, R., Bernard, F., Braat, L., et al. (2012). Global estimates of the value of ecosystems and their services in monetary units. *Ecosystem Services, 1,* 50–61.

Demirkesen, A. C. (2008). Digital terrain analysis using Landsat-7 ETM+ imagery and SRTM DEM: a case study of Nevsehir province (Cappadocia), Turkey. *International Journal of Remote Sensing, 29,* 4173–4188.

Ehrlich, P. R. (1982). Human carrying capacity, extinction and nature reserves. *BioScience, 32,* 331–333.

Ehrlich, P. R., Kareiva, P. M., & Daily, G. C. (2012). Securing natural capital and expanding equity to rescale civilization. *Nature, 486,* 68–73.

Eisfelder, C., Kuenzer, C., & Dech, S. (2012). Derivation of biomass information for semi-arid areas using remote sensing data. *International Journal of Remote Sensing, 33,* 2937–2984.

Gilmanov, T. G., Aires, L., Barcza, Z., Baron, V. S., Belelli, L., Beringer, J., et al. (2010). Productivity, respiration, and light-response parameters of world grassland and agroecosystems derived from flux-tower measurements. *Rangeland Ecology and Management, 63,* 16–39.

Haberl, H., Erb, K. H., Krausmann, F., Gaube, V., Bondeau, A., Plutzar, C., et al. (2007). Quantifying and mapping the human appropriation of net primary production in earth's terrestrial ecosystems. *Proceedings of the National Academy of Sciences of the United States of America, 104,* 12942–12945.

He, C. Y., Shi, P. J., Chen, J., Li, X. B., Pan, Y. Z., Li, J., et al. (2005). Developing land use scenario dynamics model by the integration of system dynamics model and cellular automata model. *Science in China, Series D: Earth Sciences, 48,* 1979–1989.

Jackson, R. B., Canadell, J., Ehleringer, J. R., Mooney, H. A., Sala, O. E., & Schulze, E.-D. (1996). A global analysis of root distributions for terrestrial biomes. *Oecologia, 108,* 389–411.

Jo, H.-K., & McPherson, E. G. (1995). Carbon storage and flux in urban residential greenspace. *Journal of Environmental Management, 45,* 109–133.

Jobbagy, E. G., & Jackson, R. B. (2000). The vertical distribution of soil organic carbon and its relation to climate and vegetation. *Ecological Applications, 10,* 423–436.

Kaye, J. P., McCulley, R. L., & Burke, I. C. (2005). Carbon fluxes, nitrogen cycling, and soil microbial communities in adjacent urban, native and agricultural ecosystems. *Global Change Biology, 11,* 575–587.

Lacroix, G., Lescher-Moutoué, F., & Bertelo, A. (1999). Biomass and production of plankton in shallow and deep lakes: are there general patterns? *Annales de Limnologie—International Journal of Limnology, 35,* 111–122.

Lewis, W. M. J. (2011). Global primary production of lakes: 19th Baldi Memorial Lecture. *Inland Waters, 1,* 1–28.

Li, T., Wenkai, L., & Zhenghan, Q. (2010). Variations in ecosystem service value in response to land use changes in Shenzhen. *Ecological Economics, 69,* 1427–1435.

Liu, S., Costanza, R., Troy, A., D'Aagostino, J., & Mates, W. (2010). Valuing New Jersey's ecosystem services and natural capital: A spatially explicit benefit transfer approach. *Environmental Management, 45,* 1271–1285.

Liu, H. Z., Feng, J. W., Järvi, L., & Vesala, T. (2012). Four-year (2006–2009) eddy covariance measurements of CO_2 flux over an urban area in Beijing. *Atmospheric Chemistry and Physics, 12,* 7881–7892.

Luyssaert, S., Inglima, I., Jung, M., Richardson, A. D., Reichstein, M., Papale, D., et al. (2007). CO_2 balance of boreal, temperate, and tropical forests derived from a global database. *Global Change Biology, 13,* 2509–2537.

Nowak, D., Greenfield, E., Hoehn, R., & Lapoint, E. (2013). Carbon storage and sequestration by trees in urban and community areas of the United States. *Environmental Pollution, 178,* 229–236.

Pace, M. L., & Prairie, Y. T. (2005). Respiration in lakes. In P. A. del Giorgio & P. J. L. B. Williams (Eds.), *Respiration in aquatic ecosystems* (pp. 103–122). Oxford: Oxford University Press.

Peters, E. B., & McFadden, J. P. (2012). Continuous measurements of net CO_2 exchange by vegetation and soils in a suburban landscape. *Journal of Geophysical Research: Biogeosciences, 117,* G03005.

Plutzar, C., Kroisleitner, C., Haberl, H., Fetzel, T., Bulgheroni, C., Beringer, T., et al. (2016). Changes in the spatial patterns of human appropriation of net primary production (HANPP) in Europe 1990–2006. *Regional Environmental Change, 16,* 1225–1238.

Portela, R., & Rademacher, I. (2001). A dynamic model of patterns of deforestation and their effect on the ability of the Brazilian Amazonia to provide ecosystem services. *Ecological Modelling, 143,* 115–146.

Potter, C. S., & Klooster, S. A. (1997). Global model estimates of carbon and nitrogen storage in litter and soil pools: Response to changes in vegetation quality and biomass allocation. *Tellus B: Chemical and Physical Meteorology, 49,* 1–17.

Pouyat, R. V., Yesilonis, I. D., & Nowak, D. J. (2006). Carbon storage by urban soils in the USA. *Journal of Environmental Quality, 35,* 1566–1575.

Raich, J., Rastetter, E., Melillo, J., Kicklighter, D., Steudler, P., Peterson, B., et al. (1991). Potential net primary productivity in South America: Application of a global model. *Ecological Applications, 1,* 399–429.

Rees, W., & Wackernagel, M. (1996). Urban ecological footprints: why cities cannot be sustainable—and why they are a key to sustainability. *Environmental Impact Assessment, 16,* 223–248.

Seto, K. C., Fragkias, M., Güneralp, B., & Reilly, M. K. (2011). A meta-analysis of global urban land expansion. *PLoS ONE, 6,* e23777.

Shrestha, R. K., & Loomis, J. B. (2003). Meta-analytic benefit transfer of outdoor recreation economic values: testing out-of-sample convergent validity. *Environmental and Resource Economics, 25,* 79–100.

Sobrino, J. A., Jiménez-Muñoz, J. C., & Paolini, L. (2004). Land surface temperature retrieval from LANDSAT TM 5. *Remote Sensing of Environment, 90,* 434–440.

Tallis, H. T., Ricketts, T., Guerry, A. D., Wood, S. A., Sharp, R., Nelson, E., et al. (2013). *InVEST 2.6.0 User's Guide*. Stanford: The Natural Capital Project.

Thomazini, A., Francelino, M. R., Pereira, A. B., Schünemann, A. L., Mendonça, E. S., Almeida, P. H. A., et al. (2016). Geospatial variability of soil CO_2–C exchange in the main terrestrial ecosystems of Keller Peninsula, Maritime Antarctica. *Science of Total Environment, 562,* 802–811.

Tranvik, L. J., Downing, J. A., Cotner, J. B., Loiselle, S. A., Striegl, R. G., Ballatore, T. J., et al. (2009). Lakes and reservoirs as regulators of carbon cycling and climate. *Limnology and Oceanography, 54,* 2298–2314.

TSI. (2015).Turkish Statistics Institute databases. http://www.turkstat.gov.tr/.

TSMS. (2013). Turkish State Meteorological Service Monthly Statistics. http://mgm.gov.tr/.

Turner, W. R., Brandon, K., Brooks, T. M., Costanza, R., Da Fonseca, G. A., & Portela, R. (2007). Global conservation of biodiversity and ecosystem services. *BioScience, 57,* 868–873.

UNDP. (2015). *World urbanization prospects: the 2014 revision*. New York, NY: United Nations Development Programme (UNDP).

Weng, Q., Lu, D., & Schubring, J. (2004). Estimation of land surface temperature-vegetation abundance relationship for urban heat island studies. *Remote Sensing of Environment, 89,* 467–483.

Wolman, A. (1965). The metabolism of cities. *Scientific American, 213,* 179–190.

Zhao, S., Zhu, C., Zhou, D., Huang, D., & Werner, J. (2013). Organic carbon storage in China's urban areas. *PLoS ONE, 8,* e71975.